Annals of Nuclear Medicine (2023) 37:246–254
https://doi.org/10.1007/s12149-023-01823-2

ORIGINAL ARTICLE

Multi-timepoint imaging with PSMA-targeted [^{18}F]F-Florastamin PET/CT: lesion detection and comparison to conventional imaging

Sara Sheikhbahaei[1] · Ricardo Bello Martinez[1] · Mark C. Markowski[2] · Mario A. Eisenberger[2] · Kenneth J. Pienta[3] · Diane Reyes[3] · Mary Katherine Brosnan[1] · Ergi Spiro[1] · Rehab AbdAllah[1] · Daniel P. Holt[1] · Robert F. Dannals[1] · Rudolf A. Werner[1,4] · Martin G. Pomper[1,2,3] · Michael A. Gorin[5] · Lilja B. Solnes[1,2] · Steven P. Rowe[1,2,3]

Received: 17 October 2022 / Accepted: 27 January 2023 / Published online: 1 March 2023

Abstract

Objective The aims of this study were to investigate the utility of [^{18}F]F-Florastamin, a novel prostate-specific membrane antigen (PSMA)-targeted PET radiotracer with facile radiochemistry, relative to the conventional imaging for the detection of sties of disease and evaluate the effect of multi-timepoint imaging with [^{18}F]F-Florastamin PET on lesion detectability.

Methods Eight prostate cancer patients with known or suspected recurrence who underwent [^{18}F]F-Florastamin PET/CT at 1-h and 2-h imaging time-points were included in this prospective pilot study. [^{18}F]F-Florastamin PET images were interpreted visually and quantitatively at both time points and compared with CIM.

Results [^{18}F]F-Florastamin PET was superior to CT in the detection of active osseous metastases and small-sized metastatic lymph nodes that do not fall under the anatomic imaging size criteria for metastasis. Multi-timepoint imaging showed a significant reduction in the blood pool, bone marrow and muscular uptake, and increase in liver uptake over time. There is a significant improvement in tumor-to-background ratio (TBR) at the 2-h imaging time-point ($P = 0.04$). The mean percentage change in TBR at 2-h was 21% (SD = 0.31).

Conclusions [^{18}F]F-Florastamin is a promising new radioligand for PSMA-targeted PET with suitable lesion detectability and high TBR at both time points.

Keywords [^{18}F]F-Florastamin · Prostate-specific membrane antigen PET/CT · Multi-time point imaging · Prostate cancer

Introduction

Imaging based on targeting the prostate-specific membrane antigen (PSMA) with small-molecule positron emission tomography (PET) radiotracers has revolutionized the evaluation of men with prostate cancer [1]. Recently, the United States Food and Drug Administration approved two commercially available PSMA-targeted PET imaging agents, [^{18}F]F-DCFPyL (piflufolastat F 18, PYLARIFY) and [^{68}Ga]Ga-PSMA-11 [2, 3]. Although both agents are urea-based small molecules that target the molecules main active site, there are distinct advantages to using fluorine-18 as a radionuclide in cancer imaging. These include (1) More favorable dosimetry/availability allowing for higher injected radiotracer dose; (2) Longer half-life of fluorine-18, which enables imaging at later time points resulting in higher clearance and lower nonspecific binding; and (3) Lower positron emission energy of fluorine-18 results in increased imaging spatial resolution [4–7]. Dietlein et al. demonstrated

✉ Sara Sheikhbahaei
ssheikh6@jhmi.edu

1 The Russell H. Morgan, Department of Radiology and Radiological Science, Johns Hopkins University School of Medicine, 601 N. Caroline St. JHOC Room 3233, Baltimore, MD 21287, USA

2 Department of Oncology, Sidney Kimmel Comprehensive Cancer Center, Johns Hopkins University School of Medicine, Baltimore, MD, USA

3 The Department of Urology, James Buchanan Brady Urological Institute, Johns Hopkins University School of Medicine, Baltimore, MD, USA

4 Department of Nuclear Medicine, University Hospital Würzburg, Würzburg, Germany

5 Milton and Carroll Petrie, Department of Urology, Icahn School of Medicine at Mount Sinai, New York, NY, USA

the benefits of [^{18}F]F-DCFPyL over [^{68}Ga]Ga-PSMA-11 in terms of image quality and lesion detection [6]. These data suggest that future generations of PSMA PET radiopharmaceuticals should focus on leveraging this radionuclide.

Multiple other [^{18}F]F-labeled radiotracers for PSMA PET that aim to improve upon the performance characteristics of [^{18}F]F-DCFPyL are under investigation [8]. One class of compounds incorporates large hydrophobic groups to try to take advantage of a secondary binding pocket near the PSMA active site [9]. Although a reasonable approach, this seems to lead to off-target binding in benign lesions that lack PSMA expression [10]. An alternative strategy for radiotracer development can be seen in the design of [^{18}F]F-Florastamin, which took the opposite approach of employing a minimalist hydrophilic chemical structure to drive rapid blood pool clearance and minimize off-target binding [11]. [^{18}F]F-Florastamin can be easily synthesized in high radiochemical yield through the application of click chemistry in the linker portion of the molecule.

A first-in-human study of [^{18}F]F-Florastamin found high lesion detectability and overall favorable imaging characteristics and dosimetry [11]. In this study, we aimed to investigate (1) the utility of [^{18}F]F-Florastamin in imaging prostate cancer relative to conventional imaging modalities (CIM, i.e., computed tomography, magnetic resonance imaging, bone scan) and (2) the effect of 1-h and 2-h acquisition time on lesion detectability.

Materials and methods

Patients

This prospective pilot study was approved by our local Institutional Review Board (IRB00231620) and was carried out under the auspices of a U.S. Food and Drug Administration New Drug Application (IND #147289). A total of eight patients were enrolled in the study and imaged with [^{18}F]F-Florastamin PET/CT.

Key inclusion criteria were: (1) males ≥ 18 years of age, (2) able to provide signed, informed consent and confirm that they are able and willing to comply with all protocol requirements, (3) histologically confirmed adenocarcinoma of the prostate, (4) evidence of recurrence (biochemical recurrence and/or new or progressive metastatic disease on CIM), and (5) willingness to be imaged prior initiation of new systemic therapy for recurrent and/or progressive metastatic disease. Laboratory inclusion criteria were: (1) adequate hepatic function with serum bilirubin ≤ 1.5 times the upper institutional limits of normal, (2) ALT and AST ≤ 2.5 times the upper institutional limits of normal, (3) adequate renal function with serum creatinine ≤ 1.5 times the upper institutional limits of normal, (4) adequate hematologic function with absolute neutrophil counts ≥ 1500/mm^3 and platelets ≥ 100,000/mm^3, and (5) all electrolytes must be within normal limits or judged not clinically significant by the investigator. Exclusion criteria were (1) prior administration of any radioisotope within five physical half-lives prior to study drug injection and (2) subjects with any medical condition or other circumstances that, in the opinion of the investigator, would compromise obtaining reliable data, achieving study objectives, or completion.

Radiochemistry and image acquisition

[^{18}F]F-Florastamin was synthesized adopting the two-step synthesis that has been previously published [11]. Purification by HPLC afforded the final radiotracer product in 1 mL ethanol and 14 mL normal saline. The final product passed all good manufacturing practice requirements for purity, sterility, and apyrogenicity used for PET products. The average [^{18}F]F-Florastamin specific activity at the time of injection was 63,538 mCi/μmole, resulting in approx. 0.1 μg of carrier product mass for an injected dose of 10 mCi.

Patients were imaged with a protocol appropriate for determining dosimetry. Scans were acquired on either a General Electric DVCT 64-slice scanner (GE Healthcare, Waukesha, WI, USA, 7 patients) or a Siemens Biograph mCT 128-slice scanner (Siemens Healthineers, Erlangen, Germany, one patient). The use of two different scanners mirrors the typical oncology PET workflow at our institution. Although this could have introduced an additional source of variability, a previous study in our center showed no significant variability in the mean liver uptake (SUVmean) between the two scanners [12]. Similarly, our study showed no significant difference in liver SUVmean between two scanners at different time points.

Immediately after a slow intravenous injection of 10 ± 1 mCi of [^{18}F]F-Florastamin, an initial low-dose X-ray CT transmission scan was obtained. Next, a series of four whole-body PET emission acquisitions were obtained, initially at one minute per bed position to capture blood clearance, then increased to two and then four minutes per bed position to maintain reasonable counting statistics over decay. At 120 min following the injection of [^{18}F]F-Florastamin, a second low-dose X-ray CT transmission scan was obtained followed by a PET emission acquisition, again at four minutes per bed position. The field-of-view for all scans was the mid-thighs through the skull vertex.

A total of five whole-body PET emission acquisitions were obtained for radiation dosimetry purposes, which is not the aim of the current study. We visually determined that the two later imaging time-points, obtained 1-h and 2-h following the radiotracer injection, have the highest uptake and highest conspicuity for lesion detection and were thus included in image analysis.

Image analysis

To evaluate the effect of [^{18}F]F-Florastamin uptake time on background uptake and lesion detectability, 1-h and 2-h [^{18}F]F-Florastamin PET/CT images were interpreted both visually and semi-quantitatively. Two readers, a nuclear medicine physician (RMB) and a nuclear radiologist (LBS) recorded the number and location of abnormal uptake "suspicious" or "equivocal" for sites of metastatic prostate cancer on [^{18}F]F-Florastamin PET (defined as a focal or diffuse area of increased activity above nearby background at a site outside of the normal biodistribution of radiotracer). Equivocal was defined as "equivocal radiotracer uptake in lesions that are not clearly benign" or "high radiotracer uptake in lesions that are atypical for prostate cancer". Lesions were also categorized based on the location (lymph node, bone, and prostate bed/other). Disagreement was resolved by a third reader (SPR).

Suspected sites of metastases or tumor on [^{18}F]F-Florastamin PET were also quantified using maximum standardized uptake values (SUV_{max}) corrected for lean body mass at 1-h and 2-h imaging time points. To measure background average SUV (SUV_{mean}), volumes of interest (VOI) were placed in the reference region of liver parenchyma (right lobe), ascending aorta blood pool, vertebral body not involved with disease (L3 or T12 vertebra), and within the left deltoid muscles. Tumor-to-background ratio (TBR) and tumor-to-Liver ratio (TLR) were defined as $\frac{\text{Tumor SUVmax}}{\text{Background Blood pool SUVmean}}$ and $\frac{\text{Tumor SUVmax}}{\text{Liver SUVmean}}$, respectively. The number of lesions on CIM were also recorded by one reader (RBM).

Statistical methods

Normal distribution of data was assessed using Shapiro–Wilk test. Continuous variables with normal distribution were presented as mean (standard deviation, SD), non-normal variables were as median (Interquartile range, IQR) and categorical variables as frequency and percentages. A lesion-by-lesion comparison of suspected sites of disease was carried out between [^{18}F]F-Florastamin PET and CIM. Differences in background uptake, tumor SUV_{max}, TBR and TLR at 1-h and 2-h time-points were compared using paired sample *t* test. These comparisons are presented as mean difference (standard deviation). The percentage difference in TBR at 2-h is calculated as: $\frac{TBR_{(2\,h)}-TBR_{(1\,h)}}{TBR_{(1\,h)}}$. The distribution of percentage change in TBR at the 2-h imaging time point was depicted using a histogram. Statistical significance was defined as $P < 0.05$. Data were analyzed using IBM SPSS statistics (version 26, Chicago, IL, USA).

Results

Study subject demographic and clinical information

Eight patients with prostate cancer and suspected recurrence or progression based on CIM findings were enrolled and imaged with [^{18}F]F-Florastamin PET/CT. The mean age of enrolled patients was 68.5 years (SD: 7.8; range 54–79). Patients had a median PSA level of 4.45 ng/mL (IQR: 2.3—102.5). Of the eight imaged patients, 6 (75%) had undergone prior treatment with radical prostatectomy and 5 (62.5%) had undergone prior treatment with radiation therapy. Two patients had biochemical progression without findings of disease on CIM, two patients had biochemical progression with equivocal findings on CIM, and four had findings suspicious for new or progressing metastatic disease on CIM. The median time interval between CIM and [^{18}F]F-Florastamin PET/CT was 14 days (interquartile range 20). Table 1 summarizes additional clinical characteristics of the included patients. Of eight patients, four had complete CIM including a whole-body bone scan and CT of chest, abdomen and pelvis; two had a whole-body bone scan and CT of chest; one had a whole-body bone scan and CT of abdomen and pelvis; and one had pelvis and lumbar spine MRI performed 2 months after [^{18}F]F-Florastamin PET/CT.

[^{18}F]F-Florastamin PET versus CIM

The added value of [^{18}F]F-Florastamin PET relative to CIM in each patient is described in Table 1. Overall, [^{18}F]F-Florastamin PET was superior to CT in differentiating active osseous metastases from treated sclerotic lesions (2 patients) and improved the detection of small (sub-centimeter) metastatic lymph nodes that do not fall under the anatomic imaging size criteria for metastasis (4 patients). Figure 1 shows a prostate cancer patient with biochemical recurrence, with focal intense [^{18}F]F-Florastamin uptake in normal-sized retroperitoneal lymph nodes, most consistent with nodal metastases.

Table 2 summarizes the number of detected lesions (suspicious vs equivocal) with each modality categorized by lesion type. Overall, 36 sites of PET-positive [^{18}F]F-Florastamin uptake (24 suspicious, 12 equivocal for metastatic disease) were detected on 2-h imaging including 8 osseous lesions (5 suspicious, 3 equivocal) and 13 lymph nodes (11 suspicious, 2 equivocal). Other lesions include a focal [^{18}F]F-Florastamin-avid prostatic lesion in a patient who had not undergone prostatectomy and multiple suspicious pulmonary nodules (one patient). In contrast, 31 lesions were identified on CT (22 suspicious,

Table 1 Clinical characteristics of the included patients and impact of [^{18}F]F-Florastamin PET to conventional imaging modalities

Patient	Gleason score	PSA (ng/mL)	Prior treatments	ADT at the time of imaging	CIM	Clinical context	Added value of [^{18}F]F-Florastamin PET to CIM
1	7	1.2	Prostatectomy; radiotherapy	No	Bone scan; CT CAP	Biochemical recurrence, negative CIM	Detection of small radiotracer-avid nodal metastases
2	8	2.1	Prostatectomy, nodal dissection	No	Bone scan; CT AP	Biochemical recurrence, negative CIM	Detection of radiotracer-avid sub-centimeter nodal metastases
3	7	2.5	Prostatectomy; radiotherapy	No	Bone scan; CT chest	Biochemical recurrence, equivocal CIM	Detection of radiotracer-avid pulmonary nodules (limited evaluation of sub-5 mm nodules on PET)
4	9	2.7	Prostatectomy; chemo and hormonal therapy, adjuvant radiotherapy	No	Bone scan; CT CAP	Biochemical recurrence, equivocal CIM	Detection of radiotracer-avid sub-centimeter nodal metastases
5	9	6.2	Prostatectomy; chemo and hormonal therapy, radiotherapy	Yes	Bone scan; CT chest	Biochemical recurrence, positive CIM	Confirm findings on CIM
6	9	73.6	Cryotherapy, immunotherapy, chemo and hormonal therapy	Yes	Bone scan; CT CAP	Progressive disease, equivocal CIM	Detection of radiotracer-avid sub-centimeter nodal metastases and prostate lesion
7	8	2106.6	Pelvic radiotherapy, Radium-223	No	Bone scan; CT CAP	Progressive disease (mCRPC), positive CIM	Differentiate active osseous metastases from treated sclerotic lesions (non-avid on PET)
8	7	131.4	Prostatectomy, chemo and hormonal therapy, Radium-223	Yes	MRI pelvis, lumbar spine	Progressive disease (mCRPC), positive CIM	Delineate the extent of active osseous metastases

CT CAP, CT chest-abdomen-pelvis; CT AP, CT abdomen-pelvis; CIM, conventional imaging modalities; CRPC, castration resistance prostate cancer

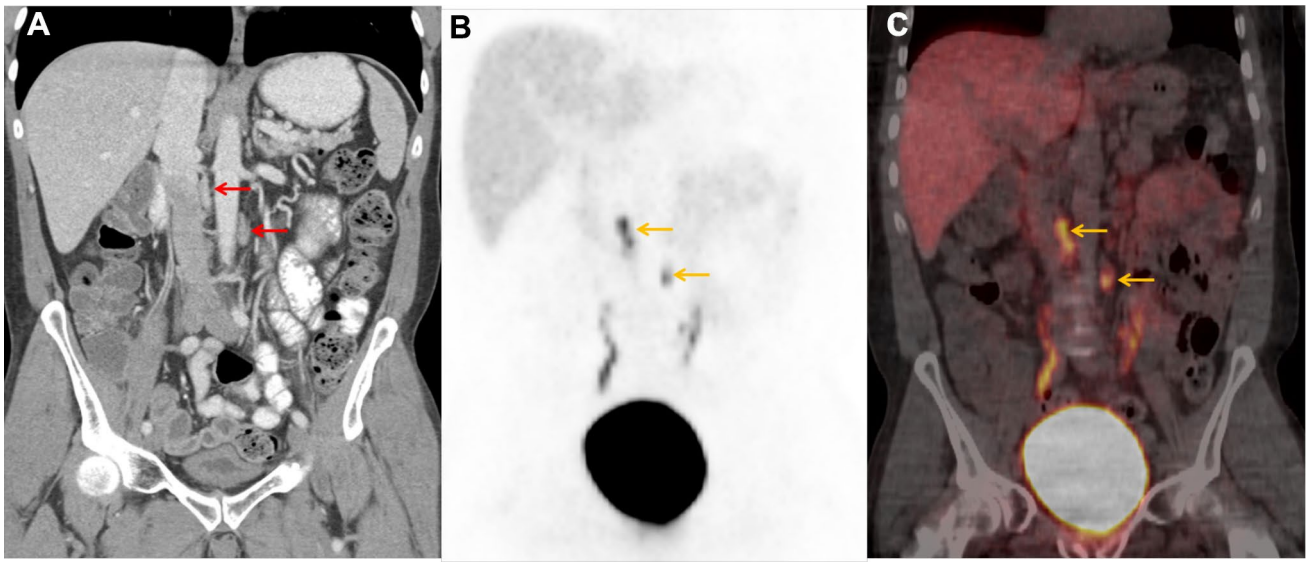

Fig. 1 **a** Coronal contrast-enhanced CT of a 54-year-old patient with prostate cancer and serum PSA of 2.7 ng/mL shows normal-sized (sub-7 mm short axis) para-aortic lymph nodes (red arrows). **b**, **c** Coronal [^{18}F]F-Florastamin PET/CT demonstrates focal intense uptake associated with retroperitoneal lymph nodes (orange arrows); physiologic excreted ureteric and bladder radioactivity is seen below the pathologic lymph nodes

Table 2 Number of lesions detected with each modality by lesion type

	All lesions		Bone lesions		Lymph node lesions		Other lesions[a]	
	Suspicious	Equivocal	Suspicious	Equivocal	Suspicious	Equivocal	Suspicious	Equivocal
[^{18}F]F-Florastamin PET/CT (1 h)	21	15	5	3	11	3	5	9
[^{18}F]F-Florastamin PET/CT (2 h)	24	12	5	3	13	1	6	8
CT	22	9	9	0	0	8	13	1
Bone scan	NA	NA	6	2	NA	NA	NA	NA

Lesions were categorized as either suspicious or equivocal

Patient #6 was not included in this table due to extensive osseous metastatic disease (too many lesions to count)

[a]Other lesions include a prostatic lesion in a patient who had not undergone prostatectomy and multiple suspicious pulmonary nodules in another patient

9 equivocal) including 9 sclerotic osseous lesions, 8 subcentimeter lymph nodes (equivocal), 1 equivocal focal lesion in the prostate gland and multiple suspicious pulmonary nodules. Of note, patient #6 was not included in this analysis as (1) extensive osseous metastases made it difficult to count the number of lesions, and (2) CIM in this patient was not comparable with other patients (pelvis and lumbar spine MRI performed 66 days after [^{18}F]F-Florastamin PET).

Multi-time point imaging with [^{18}F]F-Florastamin

On visual assessment most lesions appeared more conspicuous at the 2-h imaging time-point (Fig. 2). In two patients, several equivocal lesions at 1-h were re-categorized as suspicious at the 2-h imaging time-point (one lymph node metastasis and three pulmonary nodules). However, these additional lesions did not alter disease staging or would have led to a change in available treatment options.

Table 3 summarizes the mean difference (SD) in background uptake, tumor SUV_{max}, TBR and TLR between 2 and 1-h imaging time points. Analysis of background uptake at the 1-h versus 2-h time points demonstrated a significant reduction in the blood pool, bone marrow, and muscular uptake over time. Liver parenchymal SUV_{mean} was significantly increased at the 2-h imaging time point (mean difference = 0.41, $P = 0.02$).

There was a significant improvement in TBR at the 2-h time point, with a mean difference of 0.33 ($P = 0.04$). In an analysis based on the location of lesions, improved

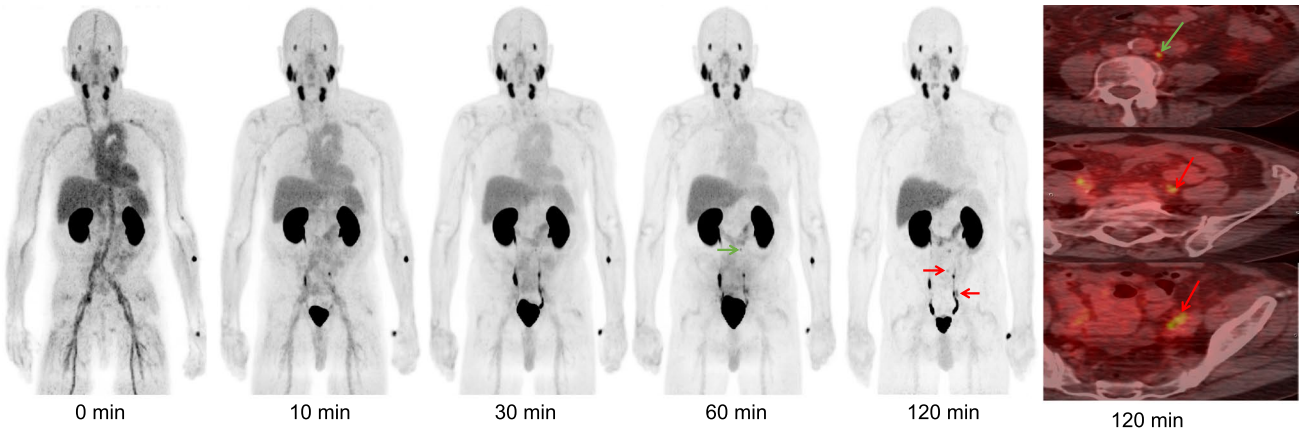

Fig. 2 Serial [^{18}F]F-Florastamin PET images of a 79-year-old prostate cancer patient with a PSA of 2.1 ng/mL. Maximum intensity projection (MIP) PET images 60 min after radiotracer injection show a focal uptake in the retroperitoneum representing a small left para-aortic lymph node metastasis (green arrow). At 2 h post-radiotracer injection, there are more conspicuous foci of uptake in the abdomen/pelvis representing additional metastases in the left common and left external iliac nodal chain (red arrows)

Table 3 Effect of time of ^{18}F-Florastamin PET/CT image acquisition on background uptake and tumor-to-background ratio

Background uptake	$SUVmean_{(2\,h)}$–$SUVmean_{(1\,h)}$	*P* value
Liver	+0.41 (0.39)	0.02*
Blood pool	−0.22 (0.11)	< 0.001*
Bone marrow	−0.16 (0.14)	0.01*
Muscle	−0.17 (0.12)	0.008*
Tumor uptake	$SUVmax_{(2\,h)}$–$SUVmax_{(1\,h)}$	*P* value
All lesions	+0.12 (0.72)	0.58
Bone	+0.18 (0.72)	0.20
Lymph nodes	−0.23 (2.21)	0.70
Others	+0.72 (1.13)	0.22
Tumor to background ratio	$TBR_{(2\,h)}$–$TBR_{(1\,h)}$	*P* value
All lesions	+0.33 (1.04)	0.041*
Bone	+0.25 (0.38)	0.004*
Lymph nodes	+0.24 (1.6)	0.60
Others	+0.99 (1.43)	0.19
Tumor to liver ratio	$TLR_{(2\,h)}$–$TLR_{(1\,h)}$	*P* value
All lesions	−0.17 (0.58)	0.051
Bone	−0.08 (0.32)	0.21
Lymph nodes	−0.45 (0.94)	0.10
Others	+0.10 (0.19)	0.28

Data presented as mean difference (standard deviation) between 2 and 1-h imaging. *P*-value < 0.05 was considered statistically significant (*)

TBR is seen at 2-h for osseous lesions but not for lymph node or other lesion types. No significant difference in values of SUV_{max} or TLR was observed between 1 and 2-h imaging. The percentage change in tumor to background uptake ratio at 2-h imaging is depicted in Fig. 3. The mean percentage change in TBR at 2-h was 21% (SD = 0.31).

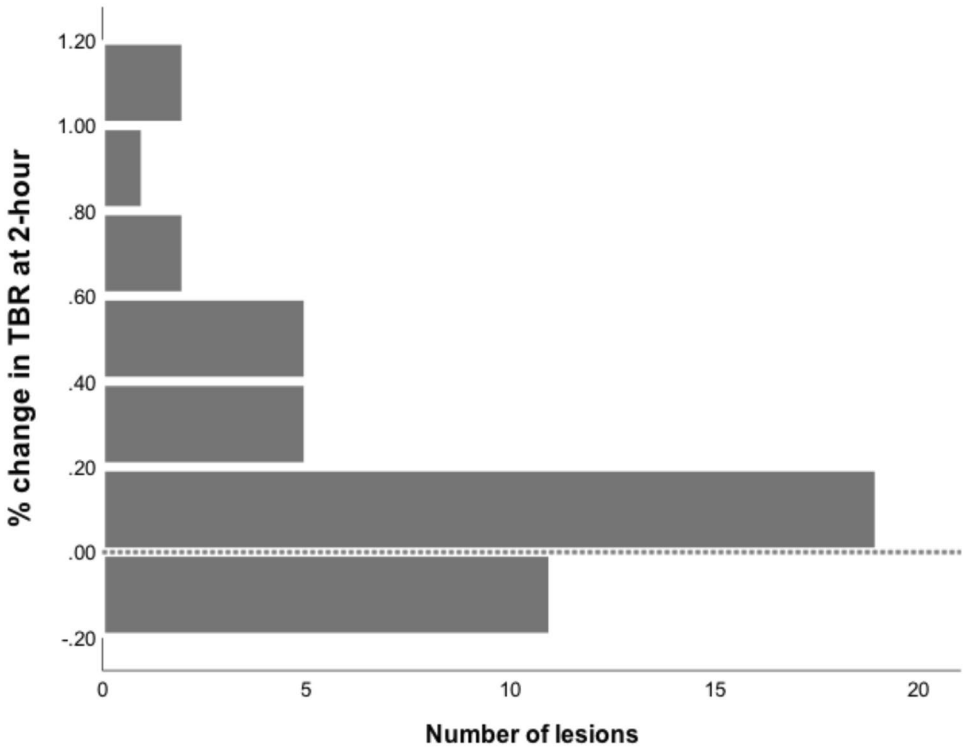

Fig. 3 The percentage change in tumor to background uptake ratio at 2-h imaging time-point

Discussion

The first-in-human trial by Lee et al. supports the feasibility and safety of PET imaging with [^{18}F]F-Florastamin. [^{18}F]F-Florastamin PET can assess PSMA expression levels with excellent specificity without significant nonspecific organ uptake, has favorable biodistribution, and provides a relatively low radiation exposure compared to other [^{18}F]F-labelled PSMA imaging agents [11]. This demonstrates that the facile radiochemistry and simple chemical structure of [^{18}F]F-Florastamin may have advantages relative to larger and more complex molecules such as [^{18}F]F-PSMA-1007.

There are multiple conclusions can be drawn regarding the results of our study. First, [^{18}F]F-Florastamin is a sensitive means of detecting sites of prostate cancer. Although the lesion detection efficiency was similar between [^{18}F]F-Florastamin PET and CIM, this would seem to at least partially reflect that some lesions visible on CIM (such as a subset of densely sclerotic bone lesions) likely reflect previously viable sites of disease that have been effectively treated. Essentially, CIM is a record of all sites of disease over time, whereas tumor-specific agents such as [^{18}F]F-Florastamin will only have uptake in sites of viable tumor.

In keeping with previously published studies [13–16], our work suggests that later imaging, at 2 h post-injection, will improve lesion visibility and background tissue clearance. Later acquisition was associated with decreased blood pool, bone marrow, and muscular background uptake and increased hepatic uptake. In our study, on visual assessment most lesions appeared more conspicuous at the 2-h imaging time-point, and few equivocal lesions at 1-h imaging were re-categorized as suspicious at 2-h. In addition, our data demonstrated significant improvement in TBR at 2-h imaging. In subgroup analysis, the difference in TBR only reached statistical significance for osseous lesions and not other lesions. However, it is important to note that the small number of patients/lesions limits the subgroup analysis, and the result should be interpreted with caution.

Several studies support the benefit of later acquisition for PSMA-radiotracers [13–15, 17]. It has been suggested that a further increase in radiotracer accumulation on late imaging can predict the likelihood of malignancy, as benign lesions usually show a decrease in SUV on late scans [18]. For PSMA radiotracers, late imaging (at 2-h for [^{18}F]F-based and at 3 h for [^{68}Ga]Ga-based tracers) offers substantial advantages and can more definitively evaluate the disease status when there is an equivocal abnormality on early images [14, 16, 17, 19–21]. Hohberg et al. showed that in patients with biochemical recurrence with low PSA levels (< 2 µg/L), [^{68}Ga]Ga-PSMA-HBED-CC PET/CT imaging 3 h post-injection frequently improved the visibility of small PSMA-positive lesions. They suggested that additional late PET imaging restricted to the lower abdomen and pelvis can be recommended when the PSA level is low without ADT [16].

Imaging at later acquisition times can reduce scanner availability; hence it can be challenging to integrate it into clinical practice. Further studies are needed to optimize

PSMA-PET acquisition protocols and determine which patients will benefit from delayed imaging.

Our study has a number of limitations. Perhaps the most noteworthy is the heterogeneity of the baseline conventional imaging. Other limitations include small sample size, heterogeneity in treatments received prior to enrollment, and lack of ground-state standard-of-truth, as histopathologic confirmation was not practically available in all patients. Our study aimed to assess the added value of [^{18}F]F-Florastamin PET/CT relative to CIM, and the effect of [^{18}F]F-Florastamin uptake time on lesion detectability, independent of the reference standard. A more fundamental evaluation of diagnostic accuracy was not the initial purpose of our study and was not feasible due to a lack of adequate reference standard. Future studies with larger sample size are needed to further elaborate the latter.

Conclusions

[^{18}F]F-Florastamin is a promising new radiotracer for PSMA-targeted PET for which there is a facile synthetic approach [22]. The agent demonstrates high TBR at multiple time points, suitable lesion detectability, and has the intrinsic advantages of radiofluorination. [^{18}F]F-Florastamin should be explored in larger studies to understand its potential role as an imaging agent for prostate cancer.

Funding We acknowledge funding for this study from FutureChem Co, Ltd.

Declarations

Conflict of interest MGP has equity in FutureChem USA, a subsidiary of FutureChem Co, Ltd.

References

1. Rowe SP, Gorin MA, Pomper MG. Imaging of prostate-specific membrane antigen with small-molecule PET radiotracers: from the bench to advanced clinical applications. Annu Rev Med. 2019;70:461–77. https://doi.org/10.1146/annurev-med-062117-073027.
2. Rowe SP, Buck A, Bundschuh RA, Lapa C, Serfling SE, Derlin T, et al. [^{18}F]DCFPyL PET/CT for imaging of prostate cancer. Nuklearmedizin. 2022;61:240–6. https://doi.org/10.1055/a-1659-0010.
3. Afshar-Oromieh A, Haberkorn U, Eder M, Eisenhut M, Zechmann CM. [^{68}Ga]Gallium-labelled PSMA ligand as superior PET tracer for the diagnosis of prostate cancer: comparison with 18F-FECH. Eur J Nucl Med Mol Imaging. 2012;39:1085–6. https://doi.org/10.1007/s00259-012-2069-0.
4. Sanchez-Crespo A. Comparison of Gallium-68 and Fluorine-18 imaging characteristics in positron emission tomography. Appl Radiat Isot. 2013;76:55–62. https://doi.org/10.1016/j.apradiso.2012.06.034.
5. Gorin MA, Pomper MG, Rowe SP. PSMA-targeted imaging of prostate cancer: the best is yet to come. BJU Int. 2016;117:715–6. https://doi.org/10.1111/bju.13435.
6. Dietlein M, Kobe C, Kuhnert G, Stockter S, Fischer T, Schomacker K, et al. Comparison of [(18)F]DCFPyL and [(68)Ga]Ga-PSMA-HBED-CC for PSMA-PET imaging in patients with relapsed prostate cancer. Mol Imaging Biol. 2015;17:575–84. https://doi.org/10.1007/s11307-015-0866-0.
7. Kuten J, Fahoum I, Savin Z, Shamni O, Gitstein G, Hershkovitz D, et al. Head-to-head comparison of (68)Ga-PSMA-11 with (18)F-PSMA-1007 PET/CT in staging prostate cancer using histopathology and immunohistochemical analysis as a reference standard. J Nucl Med. 2020;61:527–32. https://doi.org/10.2967/jnumed.119.234187.
8. Werner RA, Derlin T, Lapa C, Sheikbahaei S, Higuchi T, Giesel FL, et al. (18)F-Labeled, PSMA-targeted radiotracers: leveraging the advantages of radiofluorination for prostate cancer molecular imaging. Theranostics. 2020;10:1–16. https://doi.org/10.7150/thno.37894.
9. Giesel FL, Cardinale J, Schafer M, Neels O, Benesova M, Mier W, et al. (18)F-Labelled PSMA-1007 shows similarity in structure, biodistribution and tumour uptake to the theragnostic compound PSMA-617. Eur J Nucl Med Mol Imaging. 2016;43:1929–30. https://doi.org/10.1007/s00259-016-3447-9.
10. Dietlein F, Kobe C, Hohberg M, Zlatopolskiy BD, Krapf P, Endepols H, et al. Intraindividual comparison of (18)F-PSMA-1007 with renally excreted PSMA ligands for PSMA PET imaging in patients with relapsed prostate cancer. J Nucl Med. 2020;61:729–34. https://doi.org/10.2967/jnumed.119.234898.
11. Lee I, Lim I, Byun BH, Kim BI, Choi CW, Woo SK, et al. A microdose clinical trial to evaluate [(18)F]Florastamin as a positron emission tomography imaging agent in patients with prostate cancer. Eur J Nucl Med Mol Imaging. 2021;48:95–102. https://doi.org/10.1007/s00259-020-04883-y.
12. Sahakyan K, Li X, Lodge MA, Werner RA, Bundschuh RA, Bundschuh L, et al. Semiquantitative parameters in PSMA-targeted PET imaging with [(18)F]DCFPyL: intrapatient and interpatient variability of normal organ uptake. Mol Imaging Biol. 2020;22:181–9. https://doi.org/10.1007/s11307-019-01376-9.
13. Hoffmann MA, Buchholz HG, Wieler HJ, Rosar F, Miederer M, Fischer N, et al. Dual-time point [(68)Ga]Ga-PSMA-11 PET/CT hybrid imaging for staging and restaging of prostate cancer. Cancers (Basel). 2020. https://doi.org/10.3390/cancers12102788.
14. Rowe SP, Macura KJ, Mena E, Blackford AL, Nadal R, Antonarakis ES, et al. PSMA-based [(18)F]DCFPyL PET/CT is superior to conventional imaging for lesion detection in patients with metastatic prostate cancer. Mol Imaging Biol. 2016;18:411–9. https://doi.org/10.1007/s11307-016-0957-6.
15. Alberts I, Prenosil G, Mingels C, Bohn KP, Viscione M, Sari H, et al. Feasibility of late acquisition [^{68}Ga]Ga-PSMA-11 PET/CT using a long axial field-of-view PET/CT scanner for the diagnosis of recurrent prostate cancer-first clinical experiences. Eur J Nucl Med Mol Imaging. 2021;48:4456–62. https://doi.org/10.1007/s00259-021-05438-5.
16. Hohberg M, Kobe C, Tager P, Hammes J, Schmidt M, Dietlein F, et al. Combined early and late [(68)Ga]PSMA-HBED-CC PET scans improve lesion detectability in biochemical recurrence of prostate cancer with low PSA levels. Mol Imaging Biol. 2019;21:558–66. https://doi.org/10.1007/s11307-018-1263-2.
17. Szabo Z, Mena E, Rowe SP, Plyku D, Nidal R, Eisenberger MA, et al. Initial evaluation of [(18)F]DCFPyL for prostate-specific membrane antigen (PSMA)-targeted PET imaging of prostate cancer. Mol Imaging Biol. 2015;17:565–74. https://doi.org/10.1007/s11307-015-0850-8.
18. Alberts I, Sachpekidis C, Dijkstra L, Prenosil G, Gourni E, Boxler S, et al. The role of additional late PSMA-ligand PET/CT in the

differentiation between lymph node metastases and ganglia. Eur J Nucl Med Mol Imaging. 2020;47:642–51. https://doi.org/10.1007/s00259-019-04552-9.
19. Giesel FL, Hadaschik B, Cardinale J, Radtke J, Vinsensia M, Lehnert W, et al. F-18 labelled PSMA-1007: biodistribution, radiation dosimetry and histopathological validation of tumor lesions in prostate cancer patients. Eur J Nucl Med Mol Imaging. 2017;44:678–88. https://doi.org/10.1007/s00259-016-3573-4.
20. Afshar-Oromieh A, Sattler LP, Mier W, Hadaschik BA, Debus J, Holland-Letz T, et al. The clinical impact of additional late PET/CT imaging with (68)Ga-PSMA-11 (HBED-CC) in the diagnosis of prostate cancer. J Nucl Med. 2017;58:750–5. https://doi.org/10.2967/jnumed.116.183483.
21. Derlin T, Weiberg D, von Klot C, Wester HJ, Henkenberens C, Ross TL, et al. (68)Ga-PSMA I&T PET/CT for assessment of prostate cancer: evaluation of image quality after forced diuresis and delayed imaging. Eur Radiol. 2016;26:4345–53. https://doi.org/10.1007/s00330-016-4308-4.
22. Chen Y, Lisok A, Chatterjee S, Wharram B, Pullambhatla M, Wang Y, et al. [(18)F]Fluoroethyl triazole substituted PSMA inhibitor exhibiting rapid normal organ clearance. Bioconjug Chem. 2016;27:1655–62. https://doi.org/10.1021/acs.bioconjchem.6b00195.